



32 fraction of fluorescing aerosol particles (FAP) have repetitive daily trends when the FAP
33 fraction is positively correlated with relative humidity and negatively correlated with wind
34 speed, consistent with previous studies of fungi spores collected on substrates.

35 The results from this pilot study highlight the capabilities of ultraviolet-induced fluorescence
36 (UV-IF) measurements for characterizing the properties of FAP as they relate to daily evolution
37 of PBAPs. The use of multiple excitation and emission wavelengths, along with shape
38 detection, allows the differentiation of different PBAP types. These measurements, evaluated
39 with respect to previous, substrate-based analysis of the local fungal and pollen spores, have
40 established a starting database of measurements that future, longer term studies will build upon.

41

42

43

44

45

46

47

48

49

50

51

52

53

54

55

56

57



58

59 **1 Introduction:**

60 The formation and evolution of clouds over the tropical island of Puerto Rico have been studied
61 over the course of many years, primarily with respect to the sources of cloud condensation
62 nuclei (CCN). Puerto Rico has been the site of these studies because of its fair-weather,
63 maritime flow and mostly clean atmosphere that leads to a mountaintop cloud that forms quite
64 frequently throughout the year and can persist for several days (Allan et al., 2008; Gioda et al.,
65 2013; Spiegel et al., 2014; Valle-Díaz, et al., 2016; Raga et al., 2016; Torres Delgado, 2021).
66 In addition to the clean, maritime sources, the cloud studies have also identified particles
67 produced from upwind urban areas, both on the island of Puerto Rico as well as islands to the
68 east, where vehicular and other industrial emissions produced particles with organic carbon
69 and sulfates (Allan et al., 2008). African dust is also potentially an important source of CCN,
70 although the results are not conclusive as to how much cloud properties differ in the presence
71 of these particles (Spiegel et al., 2014; Valle-Díaz, et al., 2016; Raga et al., 2016; Torres
72 Delgado, 2021).

73 Airborne, primary biological aerosol particles (PBAP) are an important type of aerosol in the
74 tropics (Gabey et al., 2010,2013; Stanley et al., 2011) that can encompass viruses (0.01-0.3 μ m),
75 pollen (5-100 μ m), bacteria and bacteria agglomerates (0.1-10 μ m), and fungal spores (1-30
76 μ m) as well as mechanically formed particles, such as dead tissue and plant debris (Finnely et
77 al., 2017). Furthermore, there is evidence that PBAP may influence the hydrological cycle and
78 climate by initiating the ice nucleation process or acting as giant CCN (Möhler et al., 2007;
79 Pope, 2010). Upon emission from the biosphere, PBAP undergoes various physico-chemical
80 changes (coagulation, photooxidation, surface coating, etc.) and are removed through dry and
81 wet deposition. In general, biological aerosol particles, until recently, have received less
82 attention in the atmospheric science community for lack of appropriate equipment and the
83 associated measurements are expensive, labor intensive and often difficult to interpret (Cziczko
84 et al., 2006; Drewnick et al., 2008).

85 Puerto Rico has abundant plant life, e.g., a wide variety of trees, flowers, mosses and other
86 types of flora; hence, an open question is if fungal or pollen spores produced from these plants
87 might serve as CCN. The bioaerosol population in Puerto Rico, and in particular in the capital
88 city of San Juan, has been studied extensively using analysis of substrates samples (Quintero
89 et al., 2010; Rivera-Mariani et al., 2011; Rivera-Mariani et al., 2020). The objective of the



90 majority of these studies has been to evaluate the health effects of fungal and pollen spores on
91 the local population (Quintero et al., 2010; Rivera-Mariani et al., 2011; Ortiz-Martínez et al.,
92 2015; Rivera-Mariani et al., 2020). The studies by Quintero et al (2010) are particularly
93 interesting with respect to the investigation reported here because they classified a wide variety
94 of fungal and pollen spores that were the most responsible for respiratory ailments of residents
95 of San Juan. In addition, they could link the relative concentration of these spores to
96 meteorological factors. Hence, given that their studies indicated that bioaerosols are not only
97 produced in large quantities throughout the year, and highly correlated to local meteorology, it
98 is reasonable to investigate if these types of bioaerosols might also be correlated with CCN
99 measurements if such particles are hygroscopic and can easily form water droplets under the
100 right conditions.

101 Prior to embarking on a longer-term project that will evaluate PBAPs and CCN under a wide
102 range of conditions, a pilot study was designed to conduct an exploratory investigation of the
103 properties of bioaerosols and CCN during September 2019. September was selected because
104 not only did the Quintero et al. (2010) results show that this time of the year is when peak
105 concentrations of spores are found, it is also a month of frequent cloud formation.

106 In order to identify the PBAP and investigate their potential sources, we used a realtime,
107 particle by particle approach rather than a methodology that requires capturing particles for
108 offline analysis. There has been considerable progress made in the development of technologies
109 based on the working principle of ultraviolet light-induced fluorescence (UV-LIF) (Ho, 1999;
110 Huffman and Santarpia, 2017). The Wideband Integrated Bioaerosol Spectrometer (WIBS) and
111 the Ultraviolet Aerodynamic Particle Sizer (UV-APS) are examples of instruments that can
112 detect PBAP by their fluorescence, in real time, particle by particle, over a wide size range
113 (Savage et al., 2017). The WIBS and the UV-APS have been used in atmospheric bioaerosol
114 studies such as ice nucleation activity of bioaerosol (Twohy et al., 2016), measurement of
115 atmospheric fungal spore concentrations (Gosselin et al., 2016), and investigation of long-
116 range transported bioaerosol in the tropics (Gabey et al., 2010; Whitehead et al., 2016) and at
117 high altitudes (Gabey et al., 2013). The WIBS is a three channel LIF instrument developed by
118 the University of Hertfordshire and manufactured by Droplet Measurement Technologies LLC
119 available with different versions (e.g., WIBS 4A and WIBS NEO) of slightly different optical
120 and electronic configuration (Gabey et al. 2010; Perring et al. 2015). In parallel with the
121 measurement of fluorescent aerosol particles (FAP), the CCN and condensation nuclei (CN)



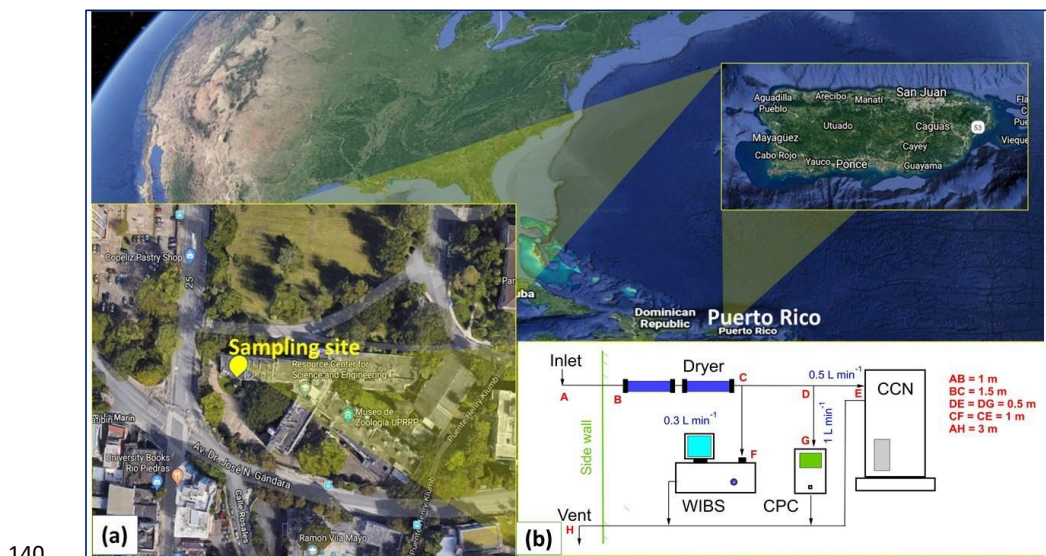
122 number concentrations were also measured in order to determine what fraction of the total
123 particle population was composed of CCN and FAPs.

124 The primary objectives of this exploratory study are to evaluate the physical properties of CN,
125 CCN and FAP, investigate correlations between CCN and FAP, analyze trends related to
126 meteorological factors, and compare the FAP measurements with those from previous studies
127 that documented fungal and pollen spores using off-line analyses.

128 2 Measurement and analysis methodology

129 2.1 Measurement site and experimental setup

130 The measurement site (Fig. 1a) is the Facundo Bueso (FB) building on the University of Puerto
131 Rico, Rio Piedras (UPR-RP) Campus (18°24'6.4"N, 66°03'6.5"W, 6 m a.m.s.l.), and for the
132 airborne spores were collected using the Hirst-type Burkard sampler (Burkard Scientific Ltd,
133 Uxbridge, UK). located on the rooftop of the Medical Sciences Campus (MSC) of the
134 University of Puerto Rico (18°23'48" N, 66°4'30" W, 60 m a.m.s.l) both located in San Juan,
135 which is the urban capital of Puerto Rico (pop. 2,448,000). San Juan has a tropical climate,
136 receiving a significant amount of rainfall throughout the year. The FB site is surrounded by
137 various sources of emission such as residential cooking, roadway traffic, and vegetation.
138 Because of the urban location, aerosol emissions from roadway traffic and nearby residences
139 contribute significantly to the total aerosol number concentrations at the site.



140



141 **Figure 1. (a) Sampling location in the FB building of UPR-RP (b) experimental setup comprising the cloud**
142 **condensation nuclei counter (CCN), condensation particle counter (CPC), and the wideband integrated**
143 **bioaerosol sensor (WIBS). This figure was generated using © Google Earth Pro 7.3.**

144 Sampling was performed for eight consecutive days (September 16-23, 2019). The
145 measurement setup consisted of two diffusion dryers (TSI model 3062) connected in series, a
146 cloud condensation nuclei counter (CCN-100, Droplet Measurement Technologies), a
147 condensation particle counter (CPC, TSI model 3772), and a wideband integrated bioaerosol
148 sensor (WIBS-NEO, Droplet Measurement Technologies) (Fig. 1b). Atmospheric aerosol
149 samples were aspirated from the exterior through the sidewall of the laboratory (~3 m above
150 the ground) with conductive tubing (1/4" internal diameter and 1 m length). The aerosols were
151 dried as they passed through two diffusion dryers (< 10% RH) containing silica gel and then
152 continued on to a manifold connected to the WIBS, CCN100, and CPC which sampled at flow
153 rates of 0.3, 0.5, and 1 L min⁻¹, respectively. Particle losses due to sedimentation, diffusion,
154 and inertial separation along the sampling lines were calculated for each of the instruments
155 (Kulkarni et al., 2011). The particle sampling efficiency with respect to particle size is shown
156 in the Supplement (Fig. S1). The sampling efficiency calculated for the particle size range 0.1-
157 3 μm is greater than 80 %. However, the sampling efficiency is reduced greatly for particle
158 sizes above 3 μm. The experimental setup allows WIBS NEO to receive particles up to 6 μm
159 with more than 60% efficiency. Due to calculation uncertainties, we have chosen not to correct
160 the data for these estimated losses because we are interested in the relative changes in the size
161 distributions with respect to time and meteorology. The absolute size of the particles is not a
162 factor in our current analysis.

163

164 **2.2 Instrumentation**

165 The CCN-100 used in this study is a continuous-flow, thermal-gradient, diffusion chamber that
166 measures the concentration of aerosols activated as cloud droplets as a function of
167 supersaturation (SS). Aerosol samples are drawn into a 50 cm tall column (inner diameter 2.3
168 cm) whose inner walls are saturated with water. A series of heaters are controlled to maintain
169 a temperature gradient from cooler to warmer as the particles move down the chamber. The
170 difference in diffusion rates between heat and water vapor creates a supersaturated environment
171 at the centerline of the cylinder. Those aerosol particles that can activate as a cloud droplet at
172 the constant SS in the chamber will begin growing as water molecules diffuse to the particle



173 surface and at the downstream of the column, an optical particle counter measures the number
174 size distribution of the cloud droplets within the size range of 0.75–10 μm . For more an in-
175 depth description of the operating principle and calibration procedures the reader is directed to
176 the paper by Roberts and Nenes (2005). In our study, the supersaturation (SS) was maintained
177 at 0.3%, a SS that is in the range of what would be encountered in convective clouds similar to
178 those that form over the island of Puerto Rico (Duan et al., 2012; Uin et al., 2016).

179 To measure the total concentration of environmental particles $> 0.01 \mu\text{m}$ we used a butanol-
180 based, condensation particle counter (CPC, model 3772 TSI) where the aerosol sample is drawn
181 continuously through a heated saturator in which butanol vapor diffuses into the aerosol stream.
182 An external vacuum pump was used to draw the aerosol samples at 1 L min^{-1} . This CPC
183 employs a single particle count mode to measure the particle number concentrations up to 10^7
184 L^{-1} at an accuracy $\pm 10\%$. The detailed design and working principle of the CPC are described
185 by Stolzenburg and McMurry (1991).

186 The WIBS measures the fluorescent characteristics of aerosols using ultraviolet, light-induced
187 fluorescence (UV-LIF) (Kaye et al., 2005; Stanley et al., 2011). This instrument provides
188 detailed information on fluorescing bioaerosols on a single particle basis. The detection
189 principles of the WIBS are discussed elsewhere (Kaye et al., 2005) and briefly described here.
190 Atmospheric particles are drawn into the WIBS via a laminar flow delivery system and pass
191 through the path of a continuous-wave diode laser (635 nm), which acts as a source for particle
192 sizing and shape detection. The total flow is approximately 2.4 L min^{-1} of which 2.1 L min^{-1} is
193 introduced in the form of sheath flow (i.e., filtered air) and 0.3 L min^{-1} is sample flow to
194 maintain the particle alignment with the 635 nm laser. The forward scattering of the light is
195 detected by a quadrant photomultiplier tube (PMT) and is used to determine the asphericity
196 factor (AF) of the particles which roughly estimates the shape of the particles (Gabey et al.,
197 2010). Experimental evidence shows that the AF is near zero for a perfectly spherical particle,
198 while it approaches 100 for a fiber or rod-like aerosol particle (Kaye et al., 2007; Gabey et al.,
199 2010). The light scattered from the diode laser is used to activate, sequentially, two Xenon
200 lamps that are filtered to illuminate the particles with UV light at 280 nm and 370 nm,
201 respectively. The wavelengths were specifically selected to excite fluorescence in particles
202 containing tryptophan (280 nm) and nicotinamide adenine dinucleotide (NADH, 370 nm). The
203 fluorescence from the 280 and 370 nm excitations is recorded by PMT detectors, one that is
204 filtered for 310–400 nm emissions and the other for 420–650 nm. Hence, when a particle is
205 excited at either of the incident wavelengths, there are four possible responses: 1) no



206 fluorescence is detected, 2) when excited at 280 nm the particle fluoresces at a wavelength in
207 the 310-400 nm waveband (FL1), 3) when excited at 280 nm the particle fluoresces at a
208 wavelength in the 420-650 nm waveband (FL2), or 4) when excited at 370 nm the particle
209 fluoresces at a wavelength in the 420-650 nm waveband (FL3). The fluorescence
210 characteristics of an individual particle are determined in any of the three fluorescence channels
211 when its fluorescence emission intensity exceeds a baseline threshold. The baseline threshold
212 is determined using the approach by Perring et al. (2015) that incorporates the daily data sets
213 to remove background artifacts. Particles that exhibit fluorescence lower than the baseline
214 threshold were treated as non-fluorescent particles. A particle that fluoresces when excited by
215 either of the xenon lamps may also produce emissions in both the 310-400 and 420-650
216 wavelength; hence, from the FL1, FL2 and FL3 signals there are seven possible combinations,
217 generally accepted by the WIBS community, that have been designated fluorescence types A,
218 B, C, AB, AC, BC, and ABC (Perring et al., 2015). Types A, B and C refer to particles that
219 fluoresce only in FL1, FL2 and FL3. The other four types are the respective combinations of
220 the A, B, and C.

221 It should be noted that A and C channels are highly sensitive to fluorescent bioaerosol particles
222 whereas the B channel is cross sensitive to non-biological aerosols (Gabey, 2011). Using the
223 fluorescence data for single particles from these three individual channels, the FAP can be
224 characterized and discriminated from non-biological aerosol particles. Based on the above
225 description, the WIBS records the optical size, particle asphericity factor (AF), fluorescent
226 excitation-emission matrix and the total number concentration (N_{WIBS}), which includes non-
227 fluorescing, and total FAP on single particle mode collected within the size range from 0.5 to
228 30 μm . Before deployment, the WIBS was factory calibrated for the size, sphericity and
229 fluorescence using reference fluorescent polystyrene latex spheres which are traceable to
230 National Institute of Standards and Technology (NIST).

231 Note, it is important to emphasize that although the WIBS was designed to detect fluorescence
232 from biological particles, it is unable to unequivocally differentiate what type of bioaerosol
233 fluoresced, e.g., if the particle was bacteria, fungus, or pollen. There are a number of studies,
234 such as those by Hernandez et al. (2016), that have used the WIBS in laboratory studies to
235 characterize a variety of species of bacteria, fungi, and pollen. Such studies have shown that
236 these three types of bioaerosols fall in general categories of size and fluorescence type. These
237 categories will be discussed further on in this paper in the context of comparing the FAP
238 characteristics in San Juan to those reported in controlled laboratory experiments.



239 The CPC measurements, taken at 1 Hz, are averaged to five minutes intervals for comparison
240 with the WIBS and CCN measurements that are also averaged in five-minute intervals. In
241 addition, the particle by particle (PbP) data from the WIBS are used to create size distributions
242 and analyze fluorescence properties and interrelationships in greater detail.

243 **2.3. Fungal spore data**

244 The fungal spore data were obtained from the department of Microbiology of the Medical
245 Sciences Campus of the University of Puerto Rico. The enumeration of outdoor spores used
246 the 12-traverse methodology proposed by the British Aerobiology Federation (Caulton and
247 Lacey, 1995). Airborne spores were collected using a volumetric Hirst-type sampler,
248 specifically a Burkard (Burkard Scientific Ltd, Uxbridge, UK). This equipment was located on
249 the rooftop of the Medical Sciences Campus of the University of Puerto Rico, 30 meters above
250 ground level. The Burkard 24-hr trapping system worked continuously with an intake of 10
251 liters of air/min. Fungal spores were impacted on a microscopic slide coated with a thin layer
252 of 2% silicon grease as a trapping surface. The slide was changed daily and mounted on
253 polyvinyl alcohol (PVA) mounting media for microscopic examination. Counting was done on
254 each preparation along 12 traverse fields every 2 hours for a total of 12 hours on the
255 longitudinal traverse. Spores were identified based on their morphological differences
256 (Quintero et al. 2010). The identification was performed by means of a bright-field optical
257 microscope NIKON Eclipse 80i microscope (Nikon Manufacturing), using a magnification of
258 1000X.

259 **2.4. Meteorological data**

260 Hourly meteorological data e.g., temperature (°C), relative humidity (RH, %), wind speed (WS,
261 m/s) and wind direction (Degree) were provided by the department of natural science taken
262 from a weather station that is ~800 m from the aerosol instrumentation.

263 **2.5. Air mass back trajectories**

264 Twenty-four-hour air mass back trajectories, ending at 100 m above mean sea level, were
265 obtained from the Hybrid Single Particle Lagrangian Integrated Trajectory Model (GDAS, 1-
266 degree resolution, HYSPLIT) to identify the possible source of the aerosols.

267

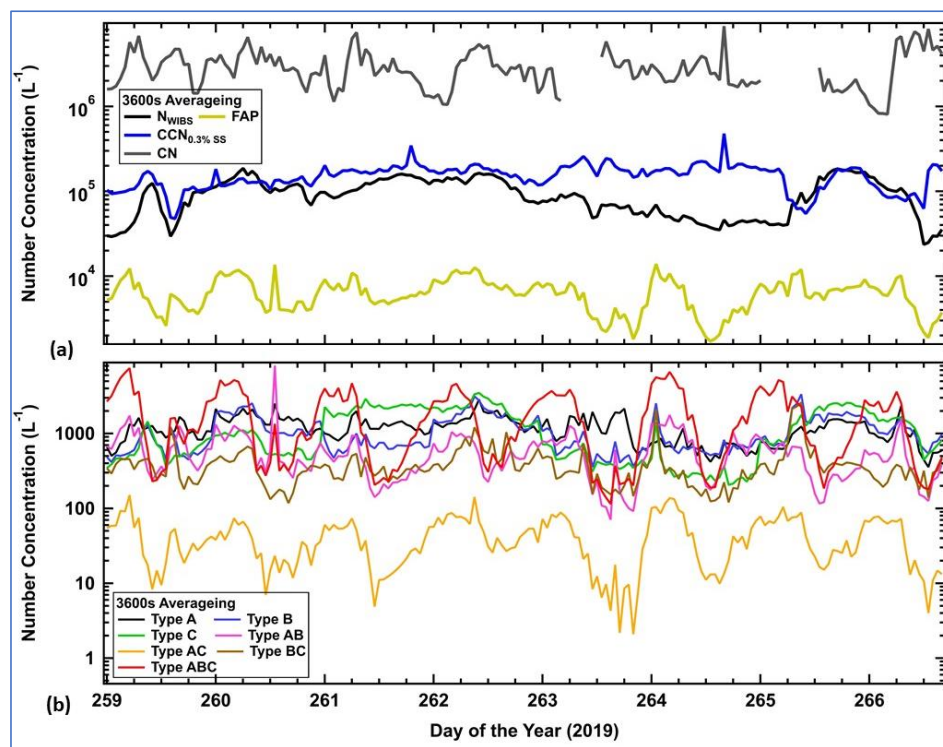
268 **3 Results and Discussion**



269 **3.1 Time series of the particle number concentrations**

270 Figure 2a shows the temporal pattern of particle number concentrations of CN, CCN (at 0.3%
271 SS) and N_{WIBS} (0.5 - 30 μm) averaged in 10-minute intervals. The average particle number
272 concentration measured by the CPC was $3\pm 1\times 10^6 \text{ L}^{-1}$. This value is higher than the CN number
273 concentrations reported previously at other more remote locations on the island, such as at the
274 northeast coastal site of the Cabezas de San Juan nature reserve and at the Pico del Este, in El
275 Yunque National Forest, where the CN concentrations were $9\pm 5\times 10^5$ and $11.6\pm 3\times 10^5 \text{ L}^{-1}$,
276 respectively, both as reported by Allan et al. (2008). The CN concentrations show systematic,
277 daily trends that reflect the motorized vehicle traffic and nearby residential emissions, the latter
278 mostly from cooking. The mean CCN concentration of $1.5\pm 0.5\times 10^5 \text{ L}^{-1}$ is about 20 times lower
279 than the CN, i.e. only about 5% of the measured aerosol particles would activate as cloud
280 droplets at a SS of 0.3%. This implies that particles over the site are mostly non-hygroscopic
281 or of low hygroscopicity.

282 The number concentrations of N_{WIBS} and FAP were $7.3\pm 5\times 10^4$ and $5\pm 3\times 10^3 \text{ L}^{-1}$, respectively,
283 which are approximately 40 and 600 times lower than the CN concentrations. Given the
284 differences in the lower size thresholds for the CPC and WIBS with respect to the smallest
285 detectable particle, 10 nm for the CPC and 500 nm for the WIBS, this implies that about 98%
286 of the particles are smaller than 500 nm. The FAP concentrations showed a systematic daily
287 cycle where nighttime particle concentrations were relatively higher than during the daytime,
288 this is being driven primarily by the type ABC FAPs as illustrated in Fig. 2b where the type
289 ABC concentrations are mostly much higher than other types. The types AB and AC
290 concentrations have trends similar to the type ABC.

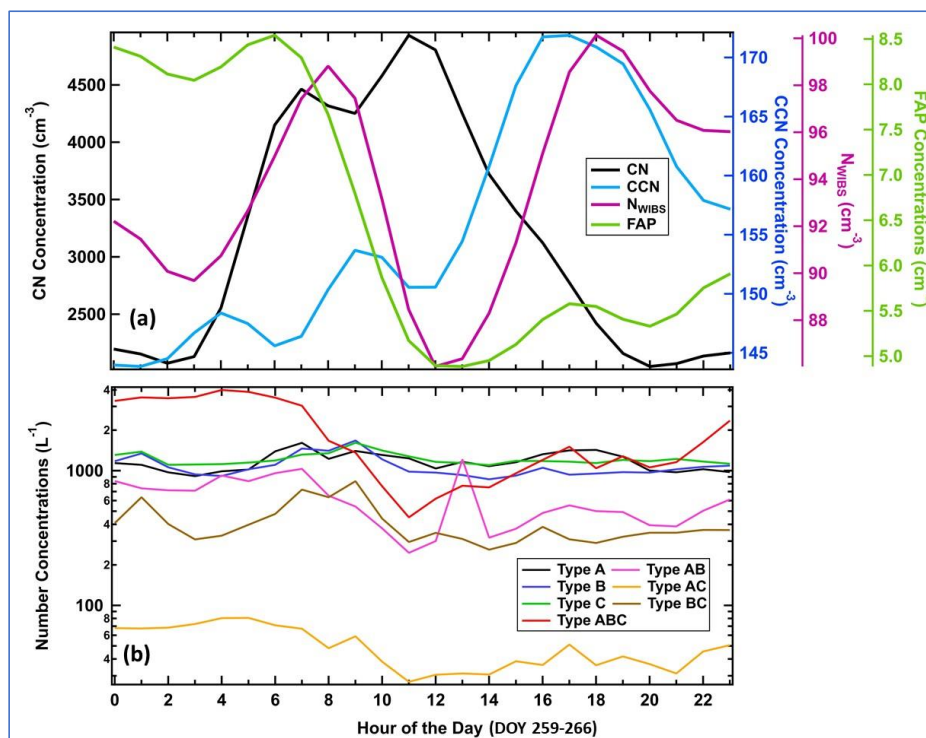


291

292 **Figure 2. Time series of the number concentrations. (a) CN, CCN, N_{WIBS} and FAP. (b) FAP types A, B, C,**
293 **AB, AC, BC, and ABC. The gaps in time of the CN concentrations were when the CPC was offline.**

294

295 In the time series of number concentrations in Fig. 2 there are what appear to be periodicities
296 in the CN, CCN and FAP. This periodicity is seen more clearly in the concentrations averaged
297 by the time of the day (over the whole measurement period) as shown in Figs. 3a and 3b. Figure
298 3a highlights the diel trend in CN concentration (black curve) that begins increasing at 4 am,
299 reaches an initial peak at 7 am, is followed by a second peak four hours later at 11 am then
300 begins decreasing the remainder of the day. The CCN concentration shows an increasing trend
301 early in the morning but doesn't start its rapid increase until midday when it begins increasing
302 until reaching its peak around 4 pm, five hours after the peak in the CN. The N_{WIBS} and FAP
303 concentrations are drawn in magenta and green, respectively. The N_{WIBS} shows an increase in
304 the morning with an initial peak at 7 am, similar to the CN; however, these concentrations then
305 decrease until peaking again in the late afternoon, an hour after the CCN peak. The average
306 FAP concentrations remain elevated between midnight and 6 am, after which they decrease by
307 about 30% and remain fairly constant the remainder of the day.



308

309 **Figure 3. (a) Hourly concentrations of CN (black curve) and CCN at 0.3% supersaturation (solid blue**
310 **curve), N_{WBS} (magenta) and FAP (green) concentrations. (b) Hourly concentrations of the seven types of**
311 **FAP.**

312

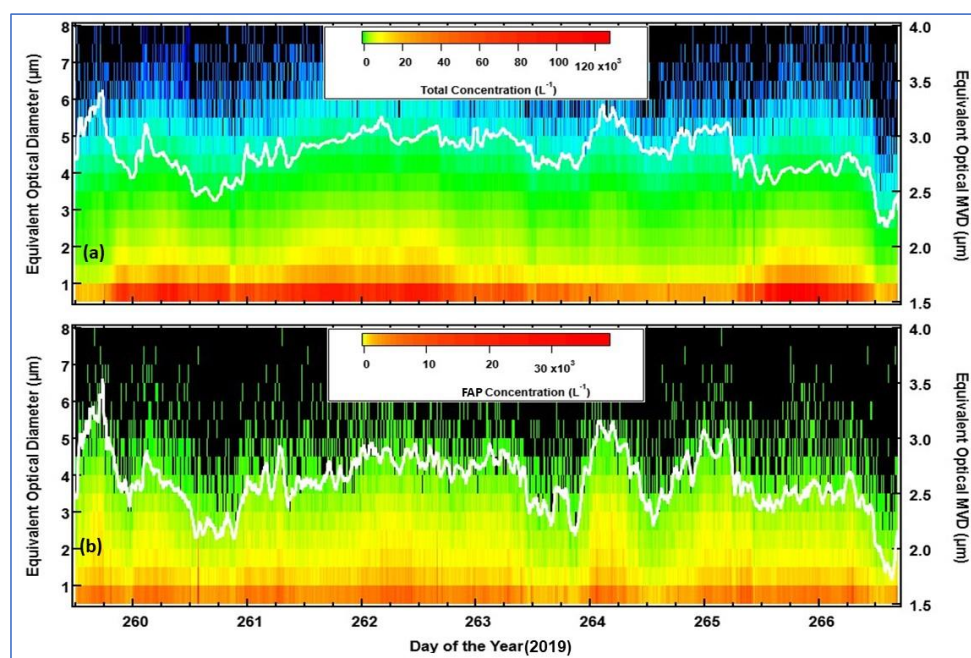
313 Figure 3b displays the hourly behavior over the averaged, 24-hour period of the seven types of
314 FAP. For all of the types except the AC and ABC, the FAPs remain relatively constant
315 throughout the day. The types AC and ABC are elevated in concentration between midnight
316 and around 6 am, both about a factor of three higher during those hours than during the
317 remainder of the day. Although the types AC and ABC follow the same trend, the type ABC is
318 about 50 times larger and dominates the FAPs during those hours. During the remainder of the
319 day, the types A, B and C are approximately equal in concentration.

320 **3.2 Temporal trends of the particle size distribution**

321 Figure 4 shows the size distributions of total (Fig. 4a) and FAP (Fig. 4b) number concentrations
322 measured from September 16 to September 23, averaged in 10-minute intervals. The color
323 scale is the log of the concentration. The white curves are the average median volume diameters



324 for the total (Fig. 4a) and FAP (Fig. 4b). The total number size distributions show an irregular
325 trend of increasing concentrations over all sizes, usually occurring around midday on all days
326 except on the day of the year (DOY) 264 when the size distributions remain approximately the
327 same throughout the day. In contrast, the FAP size distributions have a more regular, daily
328 pattern whereby the concentrations increase over all sizes to a maximum between midnight and
329 6 am.



330

331 **Figure 4.** Time series of total (a) and (b) fluorescent particle size distributions measured by WIBS for the
332 period September 16-23 (DOY 259-266), 2019. The white curves are the average median volume diameters
333 (MVD).

334

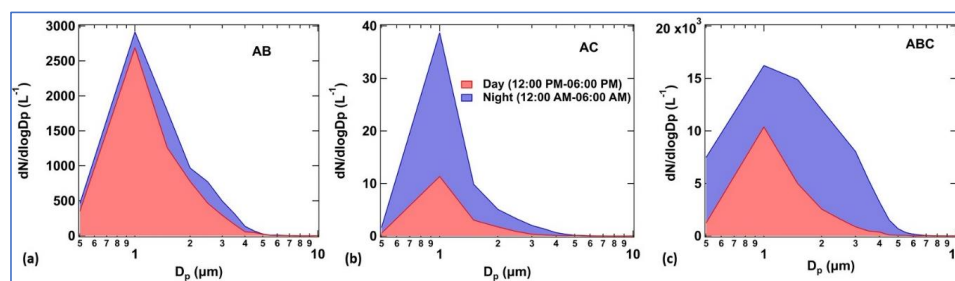
335 The daily trends of the size distributions of the seven different types of fluorescent particles
336 are shown in the Supplement (Fig. S2). where we observe that ABC and AB types were
337 dominant at the site with a unique and systematic diel cycle. Reflecting the behavior of the total
338 concentrations in Fig. 3b, the average EODs of ABC and AB type particles increase at night
339 when the particle size grows to $>4 \mu\text{m}$ by midnight. Fluorescent type A does not show any
340 specific temporal trend while types B and C have periods when the concentrations increase
341 over all sizes but do not follow the trends of the ABC and AB types particles. The type BC and
342 AC particle concentrations are much lower than the other types.



343

344 The increases in the modal diameter from daytime to nighttime, seen in the Supplement (Fig.
345 S2), particularly for the types AB, AC and ABC, was further investigated by comparing the
346 size distributions averaged at night and in the daytime. We have plotted the particle size
347 distributions for these three FAP types (Fig. 5), averaging from noon to 6 pm (red shading)
348 from midnight to 6 am (blue shading) over the whole measurement period (DOY 259-266).
349 These two periods represent time intervals when the number concentrations and average sizes
350 exhibit the largest differences. All three FAP types show a shift towards larger sizes from
351 daytime to nighttime; however, the type ABC particles have the most distinctive shifts (Fig.
352 5c), indicative of both a general increase in concentration over all sizes but a very clear, larger
353 increase proportionately at EODs larger than 2 μm .

354



355 **Figure 5.** The size distributions from types (a) AB, (b) AC and (c) ABC were averaged from 12 pm to 6 pm
356 (red shading) and from midnight to 6 am (blue shading) for the eight days of the project.

357

358 3.3 Asphericity

359 The asphericity derived from the quad detector of the WIBS is a relative indicator of the shape
360 of each particle as shown in the supplement (Fig. S3) for FAP type (AB, AC, and ABC) and
361 for all particles including the non-FAP. The color scale shows the average asphericity at each
362 size interval over the duration of the project. Among the fluorescent types, the asphericity of
363 ABC particles shows a mode between 2 and 4 μm during nighttime, especially at midnight.
364 The asphericity size distributions of all particles show a broader mode of enhanced asphericity
365 between 2 and 4 μm that varies somewhat but not in a noticeable diel pattern. Note that particles
366 with asphericities < 20 are generally considered quasi-spherical so that the values that are
367 shown here indicate slight changes in shape, on average, of type ABC particles, as well as all
368 particles, but the overall population of particles can be considered quasi-spherical.



369 Asphericity of non-fluorescent (non-FAP) particles was always observed higher than the FAP
370 (Fig. S3d in the Supplement). The higher values of asphericity of non-FAP particles can be
371 seen between size 3 and 6 μm every day and dominate on DOY 261 and 262.

372 **3.4 Air mass back trajectories**

373 Air masses arriving at the site on DOY 259 and 264 were coming from the northeast of the
374 island originating 24-hours earlier over the Atlantic Ocean. The air masses that arrived on DOY
375 260-63 and 266 were from the southeast of the island and on DOY 265 the air was from the
376 south-southeast. Figure S4a shows that all of the air masses had been < 50 m above the surface
377 the entire 24-hour period before arriving at the measurement site. The one exception was on
378 DOY 259 when the air mass had stayed above 200 m from 12 to 24 hours then began
379 descending as it approached the island. This same air mass was associated with rain formation
380 close to the measurement site (Fig. S4b in the Supplement). The air mass on DOY 264 came
381 across the islands to the SE of Puerto Rico (e.g., Culebra and the British Virgin Islands),
382 possibly mixing the marine aerosols with polluted emissions before arriving at the
383 measurement site. Likewise, the air mass trajectory on DOY 260 and 262 crossed over the
384 Vieques and US Virgin Islands at a low altitude, likely mixing with anthropogenic emissions.
385 The air mass arriving on DOY 261 is comparatively dry as no rainfall happened along its
386 trajectory, but it also crossed over the Vieques island. The remainder of the air masses were
387 presumably not impacted by anthropogenic emissions until arriving over the Puerto Rico
388 landmass.

389 **3.5 Meteorological data**

390 Figure S5 shows the temperature and relative humidity (RH) (Fig. S5a in the Supplement), and
391 the wind speed, wind direction and precipitation (Fig. S5b in the Supplement). The average
392 wind speed, temperature, and RH for the period of measurement were 2.8 ± 2.4 m/s, 29 ± 2 °C,
393 and 77 ± 11 %, respectively. The DOYs 259 and 265 received significant rainfall of 1.35 and
394 1.84 inches, respectively. Note that these two days are also those that the back trajectory
395 analysis indicated that rain had formed in the arriving air masses. The wind speed and direction,
396 temperature, and RH show a systematic daily cycle where the wind speed and temperature
397 peaked during midday (2.8 ± 0.7 m/s and 33 ± 1 °C), and the RH peaked around midnight (91 ± 3
398 %). Wind profiles at the measurement site show that the air was flowing from 135° - 250° during
399 the night then from 93° - 134° during the daytime. On DOY 262 and 265, as well as the afternoon
400 of DOY 259, the winds are comparatively low. The average wind speeds at night (0.24 ± 0.2

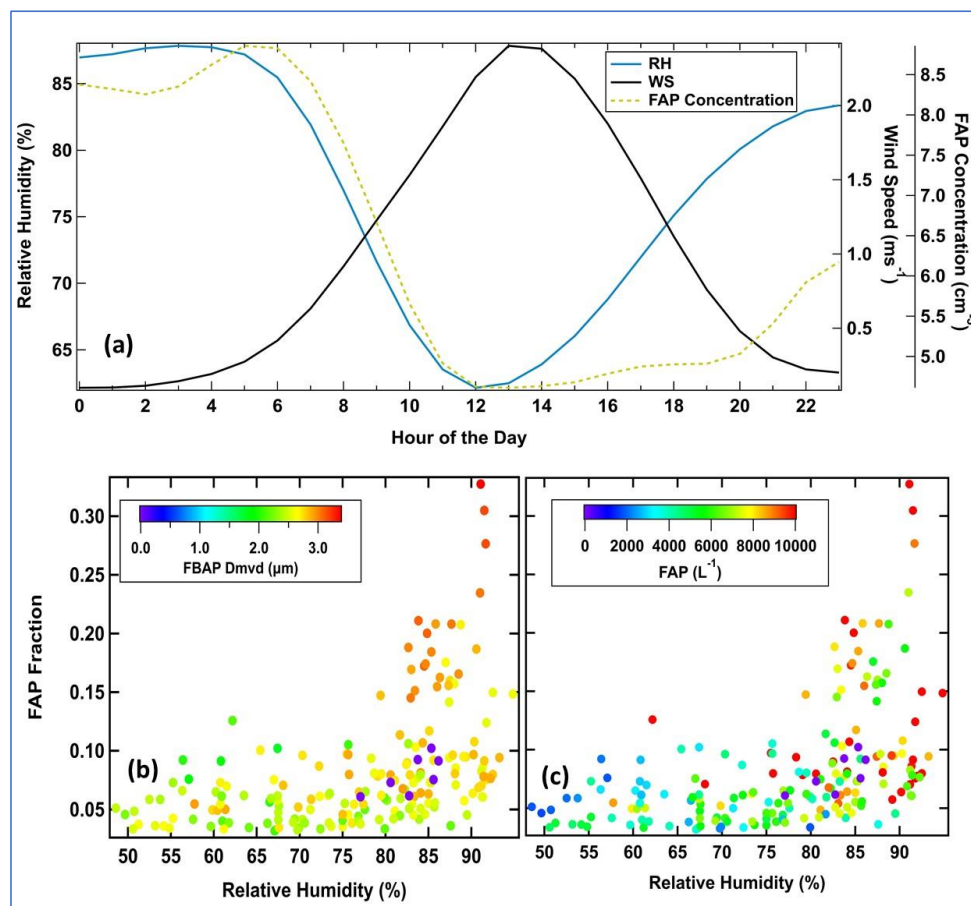


401 m/s) compared to those during the day (2.8 ± 0.6 m/s) suggest generally calm wind conditions
402 that are normal this time of year when not under the influence of tropical storms.

403

404 To further highlight the relationships between the meteorological conditions and FAP, we
405 computed the hourly averages of RH, wind speed and FAP concentrations during each 24-hour
406 period over the eight-day period and compared them in Fig. 6a. The RH and FAP
407 concentrations are maximized during the hours from midnight to 6 am while wind speed is at
408 a minimum during those hours, maximizing a little after midday.

409 The relationship between RH and the FAP fraction is further underscored in Fig. 6 where there
410 appears to be an RH threshold below about 80% that the FAP fraction remains below 0.1 but
411 then increases rapidly to greater than 0.3 as the RH exceeds 90%, i.e. less than 10% of the
412 particles measured in the size range of the WIBS were FAP when the $RH < 80\%$, but increases
413 to more than 30% at high humidities. The difference between Fig. 6b and 6c are how the
414 markers are color coded. In Fig. 6b, the coloring denotes the equivalent median volume
415 diameters (D_{mvd}) and in Fig. 6c, the coloring is the FAP concentration. Both the D_{mvd} s and
416 concentrations increase with increasing humidity and FAP fraction.



417

418 **Figure 6.** (a) hourly averages of relative humidity (blue curve), wind speed (black) and FAP concentration
419 (green dotted). (b) link between fluorescent fraction and relative humidity (FAP particle volume weighted
420 equivalent optical diameter, D_{mvd} , on the color scale). (c) fluorescent fraction and relative humidity (FAP
421 particle concentration on the color scale). The data in all the figures averaged over DOY 259-266.

422

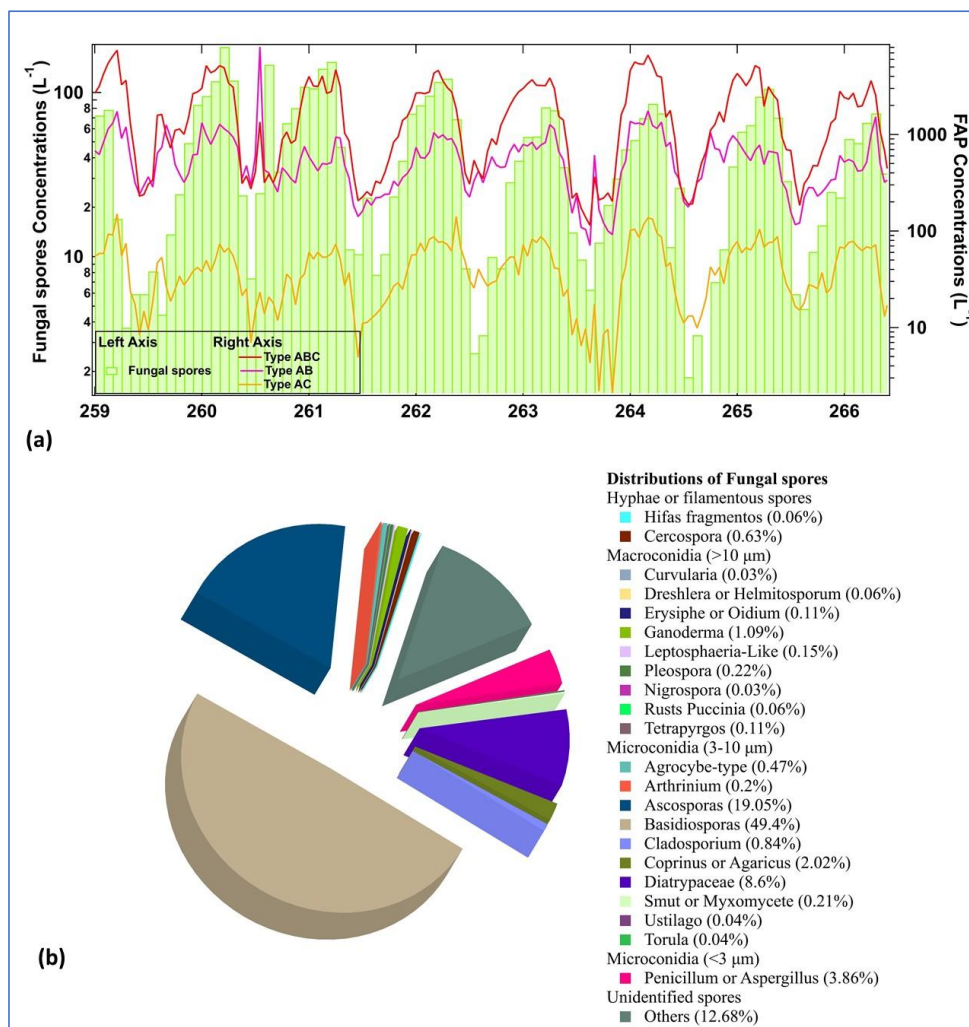
423 3.6. Fungal spore data

424 The time series of the fungal spores, measured on the rooftop of the medical science building
425 at the university, are shown in Fig. 7. Similar to the FAP number concentration and fraction,
426 the spore concentrations have a diel trend with maxima around midnight. The average
427 concentrations were $48 \pm 42 \text{ L}^{-1}$ with a maximum $112 \pm 44 \text{ L}^{-1}$ around midnight. We calculated
428 positive correlations of 0.7, 0.47, and 0.54 between the total spore concentration and
429 concentrations of FAP types ABC, AB, and AC types, respectively. Previous studies for this



430 region reported the most common fungal genera detected were the Basidiospores and
431 Ascospores (Quintero et al., 2010; Rivera-Mariani et al., 2011). Figure 7b illustrates the
432 distributions of outdoor fungal spore types recorded at MSC of the University of Puerto Rico.
433 Fungal species were identified and distributed different categories, referred to as hyphae or
434 filamentous spores, macroconidia $>10\ \mu\text{m}$, microconidia $3\text{--}10\ \mu\text{m}$, microconidia $<3\ \mu\text{m}$, and
435 unidentified spores presented in others category. We observed that the microconidia $3\text{--}10\ \mu\text{m}$
436 contributed the highest (81%) fraction to the total fungal species followed by microconidia (<3
437 μm) 3.86% and Macroconidia ($>10\ \mu\text{m}$) 1.8%. We observed that the Basidiospores contributed
438 the highest (49.4%) fraction to the total fungal spores type followed by Ascospores 19%,
439 Diatrypaceae 8.6% and Penicillum/Aspergillus 3.86%. The mean concentrations of dominant
440 species such as Basidiospores, Ascospores, Diatrypaceae and, Penicillum/Aspergillus were
441 24 ± 20 , 9.3 ± 4 , 4 ± 3 and $2\pm 1\ \text{L}^{-1}$ during the study period. The Ascospores and
442 Penicillum/Aspergillus had more elevated concentrations during the night while Diatrypaceae
443 concentrations were generally higher during the daylight hours.

444 These species were the most common airborne spores in San Juan, present throughout the year
445 and predominated during September (the rainy month). The WIBS's ABC and AB types were
446 likely the Basidiospores and Ascospores (Fig. 7b). The other genera most frequently detected
447 were the Penicillium/Aspergillus, Cladosporium and Ganoderma, present at low concentrations
448 reported by Quintero et al. (2010). Those species possibly corresponded to WIBS's AC types
449 which were systematic and relatively low concentrations. These fungal spores, present between
450 the midnight and early morning period, suggest an active release mechanism induced by the
451 increased humidity under calm wind conditions, in concordance with the findings reported by
452 Quintero et al. (2010).



453

454 **Figure 7. (a) time series particle number concentrations of fungal spores (left axis) measured at the Medical**
 455 **science department and the FAP types ABC, AB and AC (right axis) detected by WIBS at FB site. (b)**
 456 **distributions of outdoor fungal spores recorded at Medical Sciences Campus, San Juan.**

457

458 4. Discussion

459 From the results presented above, the following features stand out: 1) The CN, CCN and FAP
 460 concentrations have daily patterns during which each maximizes at a different hour of the day,
 461 2) the periodic FAP concentration is predominantly of the type ABC that reaches a daily
 462 maximum around midnight and the asphericity of this type of FAP increases slightly during



463 the same time period, 3) the RH reaches a maximum each day around midnight, 4) the wind
464 speeds are a minimum around midnight and 5) an independent analysis of bioaerosols using
465 fluorescence microscopy to identify spore types revealed a periodicity of spore concentrations
466 that was highly correlated with the RH and FAP type ABC concentrations.

467 Referring back to Fig. 3a, the CN, CCN, N_{WIBS} , and FAP concentrations all exhibit a diel
468 periodicity but with peak values occurring at differing hours. The CN population encompasses
469 all environmental particles larger than about 10 nm and are dominated by anthropogenic
470 aerosols, i.e., those produced from residential cooking and local vehicular traffic. Given that
471 the WIBS measures the concentration of particles larger than $0.5\mu\text{m}$, and that the total
472 concentration has an average peak maximum of 100 cm^{-3} , compared to a maximum CN
473 concentration 5000 cm^{-3} , this implies that 98% of the particles have sizes smaller than $0.5\mu\text{m}$.
474 A comparison of the maximum CCN and N_{WIBS} concentrations, 170 cm^{-3} vs 100 cm^{-3} , leads us
475 to conclude that most of the CCN are in sizes greater than $0.5\mu\text{m}$. Likewise, since the maximum
476 CCN concentrations are only about 2% of the CN values, this suggests that most of the CN
477 have low hygroscopicity, a characteristic of fresh combustion particles.

478 The trends in the CN concentrations suggest that there are early morning activities that are
479 producing emissions of anthropogenic particles. The two peaks are a result of the combination
480 of two traffic patterns: the general city traffic as workers commute to jobs that are not on the
481 university campus and vehicular traffic of university workers whose starting hours are later
482 than the city workers. In Fig. 1a, the sampling site is located near the intersection of two major
483 streets that carry both types of traffic. Unlike many large urban areas where morning and
484 evening rush hour traffic can be distinctly seen in the CN measurements, there is a smaller
485 density of cars during the evening commute than in the morning in San Juan.

486 The correspondence between the times of the two N_{WIBS} maxima and the CN and CCN peaks
487 suggests that the $> 0.5\mu\text{m}$ particles measured with the WIBS in the morning are a different
488 mixture of compositions than the particles in the afternoon. The morning N_{WIBS} peak lags the
489 first CN peak by an hour, likely as result of the primary emissions producing particles that grow
490 into the size range of the WIBS; however, with the sunrise at around 6 am, temperatures begin
491 increasing and the material in the more volatile particles begin to evaporate until the particle
492 sizes decrease below the threshold of the WIBS. Some dilution will be occurring as the
493 boundary layer deepens with increasing temperatures, but this is a secondary effect as we do
494 not see the CN concentrations decrease with the decrease in N_{WIBS} . Since the CCN



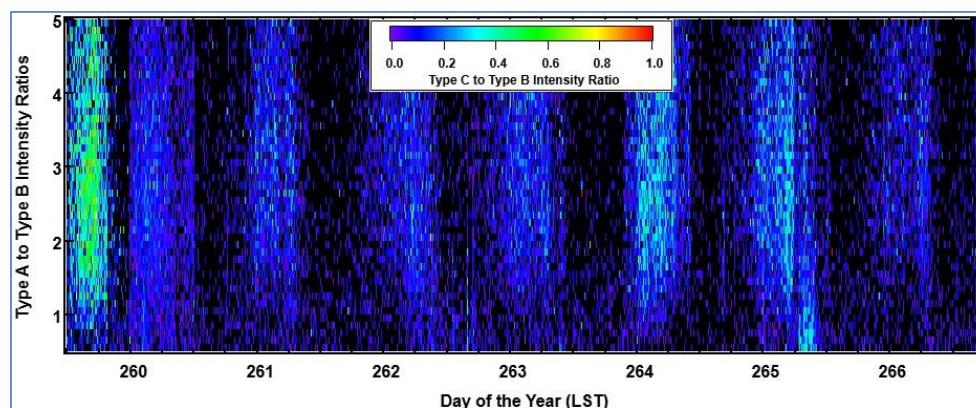
495 concentrations remain low during this period, this implies that either the particles did not grow
496 large enough to be good CCN or their composition is non-conductive for forming CCN. In the
497 early afternoon we observe the CCN concentrations beginning to increase until reaching their
498 late afternoon peak. The N_{WIBS} follows a very similar trend but lagged with respect to the CCN
499 by a couple of hours. This afternoon trend in CCN has been identified in other large, polluted
500 urban areas as the result of photochemical reactions producing hygroscopic, secondary organic
501 aerosols (SOA) from photochemical reactions (Baumgardner et al., 2004). The N_{WIBS} is offset
502 a couple of hours due to the time needed for the SOA particles to grow by condensation and
503 aggregation. Finally, the FAP concentrations only begin increasing late in the evening after the
504 CCN has maximized and their concentrations are less than 10% of the CCN. This suggests that
505 if FAP are good CCN, they do not contribute significantly to the overall CCN population.

506 Quintero et al. (2010) concluded that the release of the fungal spores that they measured and
507 speciated was triggered by high RH and were found in multiple locations. Pollen spores, on the
508 other hand, could not be linked conclusively to any meteorological factor. Hence, given these
509 previous results in comparison with the correlations that we have observed in the current study
510 (Figs. 6 and 7), the type ABC fluorescing particles are most clearly linked to Basidiospores and
511 Ascospores, the two species that made up the largest fraction of fungi measured with the
512 fluorescence microscopy. The hourly averages in Fig. 3b also showed that the type ABC only
513 was predominant during the same period as the Basidiospores and Ascospores but then the
514 other fluorescence types A, B and C were equally present during the remainder of the day. This
515 is mirrored by the spore types shown in Fig. 7 that change in relative mixture during the day.
516 Hence, by observing the relative changes in the seven FAP types, we get a qualitative measure
517 of the changing population of bioaerosols.

518 The WIBS characterizes the fluorescent aerosol particles using two-wavelength excitations and
519 two-wavelength emissions. The sensitivity of types A and B to the intensity of the emissions
520 in the 310–400 and 420–650 nm wavelength bands, when excited at 280 nm, in comparison to
521 the intensity of emissions at 420–650 nm when excited at 370 nm has been exploited in the
522 study by Ziemba et al. (2016) to identify differences in bioaerosol types as they relate to
523 differences in FAP sources. In their study they were able to show a clear grouping of FAPs
524 linked to source regions by plotting the ratio of type A to type B (emission sensitive) versus
525 the ratios of type C to type B (excitation sensitive). We have followed a similar scheme;
526 however, whereas the Ziemba et al (2016) study used a WIBS on an airborne platform flying
527 over various land usage types, our site was fixed so we compute these ratios as a function of



528 time rather than location. Figure 8 illustrates the periodicity of the type C to B ratio, increasing
529 during those time periods that the type ABC concentrations were also increasing. Just as the
530 sizes of FAP were seen to increase during these periods (Fig. 5), indicative of a change in FAP
531 type, the shift in the type C/type B reflects the differences in the fungal spore types.



532

533 **Figure 8: Temporal distribution of emissions wavelength dependence (Type A to Type B) vs excitation**
534 **wavelength dependence (Type C to Type B).**

535

536 Hence, the changes in size distribution, asphericity, type C/B ratios, and speciated spore
537 concentrations, all occurring during the same time of day, provide independent verification that
538 a different type of PBAP is being produced during the periods of high RH than during the other
539 periods of the day.

540 The strong correlation between spore release and RH that has been highlighted in this study
541 has been previously reported, e.g., (Oliveira et al., 2005; Chi and Li, 2007; Gabey et al., 2013;
542 Calvo et al., 2018, Toprak and Schnaiter, 2013; Healy et al., 2014). None of those studies,
543 however, were from tropical regions nor they include the asphericity and FAP type rationing
544 to quantify their results.

545 Some laboratory studies have been conducted to measure the fluorescence characteristics of a
546 small variety of bacteria, fungi, and pollen, for example Hernandez et al. (2016) determined
547 that bacteria, fungi and pollen could be generally grouped according to the size and FAP type.
548 In their study, very few fungal spores were of the FAP type ABC such as found in the current
549 study. Instead, the majority of their fungi were types A and AB while the majority of type ABC
550 spores were pollen, not fungi. On the other hand, the Hernandez et al. (2016) study did not test



551 any of the major fungi species that were measured in the natural environment of Puerto Rico,
552 i.e. Basidiospores and Ascospores.

553

554 **5. Summary and Conclusions**

555 A pilot study was conducted to evaluate the fluorescence and cloud condensation nuclei (CCN)
556 properties of urban aerosols in San Juan, Puerto Rico, the first time such measurements have
557 been made in this tropical city. Previous CCN measurements have been made on this island at
558 coastal and rainforest sites, but no research has been pursued to see if bioaerosols are directly
559 linked to CCN. There have been a number of laboratory studies conducted by other researchers
560 who evaluated the CCN activity of various bacteria, fungi and pollen. Although some types of
561 bioaerosols were found to be potential CCN, many others were not. Hence, the importance of
562 bioaerosols as cloud forming particles remains an open question. The very large concentrations
563 of fungal spores produced by flora in Puerto Rico, as reported by Quintero et al. (2010), along
564 with the results from our pilot study, provided the initial motivation for the study reported here
565 to assess if bioaerosols might contribute to the frequent cloud formation over the island.

566 The measurements were made from the Facundo Bueso building within the University of
567 Puerto Rico, Rio Piedras Campus, from September 16-23, 2019, an urban location that
568 experiences emissions from local residential cooking, vehicular traffic and a wide variety of
569 flora. The site is located close to the intersection of two major streets carrying local business
570 as well as university traffic.

571 In the pilot experiment, the CCN concentrations were measured with a commercial CCN
572 spectrometer set at 0.3% supersaturation and the fluorescent properties were also measured
573 with a commercial instrument, the Wideband Integrated Bioaerosol Spectrometer (WIBS). It
574 is important to note that bioaerosols are not the only type of aerosol particle that will
575 autofluoresce when excited at the wavelengths used in the WIBS, although care was taken to
576 minimize interference from non-biological particles. Therefore, what is reported in the current
577 study are the properties of fluorescing aerosol particles (FAP) without specifically labeling
578 them as biological. In addition to measurements of CCN and FAP, the total concentration of
579 condensation nuclei (CN) was documented with a condensation particle counter.

580 The mean number concentration measured by the CCN counter at 0.3% SS was (1.5 ± 0.5)
581 $\times 10^5 \text{ L}^{-1}$, which was about a factor 21 lower than the average CN concentration $(3 \pm 1) \times 10^6 \text{ L}^{-1}$



582 ¹. The mean FAP concentration was $(5 \pm 3) \times 10^3 \text{ L}^{-1}$, which was a small fraction (~7%) of total
583 aerosol particle number concentration, N_{WIBS} , measured by the WIBS, whose lower size
584 threshold is $0.5 \mu\text{m}$.

585 The CN, CCN, N_{WIBS} , and FAP concentrations all have diel trends but their maxima occur at
586 varying hours of the day. The CN peaks at 6 am and 11 am due to business traffic and university
587 traffic that have different rush hours. The CCN reaches its maximum value at 4 pm as
588 photochemical processes produce secondary organic aerosols (SOA) that are hygroscopic in
589 composition. The N_{WIBS} is bimodal with the morning peak at 8 am, reflecting rush hour
590 emissions whose particles grow into the size range of the WIBS and then the second maximum
591 at 6 pm as the SOA grow to measurable sizes. The diel trends in the FAP concentrations are
592 not correlated with the CN, CCN or N_{WIBS} as they remain fairly constant throughout the
593 daylight hours but then rapidly increase to their maximum value that extends from midnight
594 until 6 am.

595 The FAP are classified according to the wavelength at which they were excited and wavelength
596 at which they emitted fluorescence. These types have been categorized as A, B, C, AB, AC,
597 BC, and ABC. In the current study the types A, B, C and ABC all had average concentrations
598 during the daylight hours of about 1000 L^{-1} while the other three types were much lower in
599 concentration; however, only the type ABC showed the rapid increase in concentration, to
600 almost 5000 L^{-1} , between midnight and 6 am.

601 Independent measurements using fluorescent microscopy of spores captured on substrates were
602 made during the same time period. Although more than 20 species of spores were identified
603 with this technique, the fungi Basidiomycetes and Ascomycetes were not only the most
604 predominant, but they were also the spores that followed an almost identical diel trend as the
605 type ABC FAP, i.e. remaining nearly constant in concentration during the daylight hours then
606 increasing in the evening to their maxima between midnight and 6 am.

607 The other environmental parameters that also correlated significantly with the temporal trends
608 in fungal spores and FAP were the relative humidity (RH) and the wind speed. As the RH
609 began to increase in the late afternoon, the spore counts and FAP concentrations began
610 increasing as well. A comparison of RH with FAP concentrations indicates that the FAP
611 concentrations begin increasing above an RH threshold of about 80%. Spores are released by
612 a number of species of fungi when the RH increases, as has been well documented in other



613 studies (Quintero et al., 2010). Hence, the relationship between RH, Basidiomycetes and
614 Ascomycetes and the type ABC FAP has been clearly established.

615 Three additional properties of the FAP were extracted from the WIBS measurements that
616 provided indirect but complementary information that showed how the type ABC particles
617 were related to the Basidiomycetes and Ascomycetes: 1) the size distribution, 2) the asphericity
618 and 3) the excitation and emission sensitivity parameters. The type ABC particles during the
619 high RH periods had much higher concentrations of particles larger than 2 μm when compared
620 to the size distributions of these particles in the daylight hours. Secondly, the asphericity
621 increased during the high type ABC concentration period. Thirdly, excitation sensitivity
622 parameters increased during this same period. While not quantitative, these three parameters
623 confirmed that the particles whose concentrations were increasing had different properties than
624 during other periods of the day.

625 The trend in the CCN concentration was not directly correlated with the FAP, so we cannot
626 conclude that bioaerosols are a potential source of cloud forming particles. In addition, the FAP
627 concentrations were less than 10% of CCN concentrations, so even if some FAP are potential
628 CCN, the clouds that develop over the island are more likely formed from marine aerosols
629 rather than locally produced fungal spores.

630 The results from this pilot study have provided strong motivation for longer term measurements
631 that will expand the database of aerosol particle properties in a tropical, urban area. The detailed
632 information on fungal spores in this region, in comparison with the multi-parameter data
633 available from the WIBS, will improve our ability to interpret these measurements of FAP and
634 apply this knowledge to data sets acquired in other parts of the world.

635 **Data availability**

636 Data used to support the findings in this study have been uploaded and are publicly available
637 via Mendeley at <https://data.mendeley.com/datasets/t26dctfk7t/1> (Sarangi et al., 2021).

638 **Author Contribution**

639 BS designed the study in consultation with OLMB and performed the measurements. BBR
640 performed the measurements of fungal spores and pollen concentrations. DB and BS performed
641 the analysis, interpreted the results and wrote the paper with contributions from OLMB and
642 BBR.



643 **Acknowledgements**

644 This research was supported by NSF MRI grant (1829297) and NSF EAR Grant (1331841).
645 The authors acknowledge the Droplet Measurement Technologies, Inc., Boulder, Colorado for
646 providing training on instruments that are part of the NSF MRI project. The authors gratefully
647 acknowledge the NOAA Air Resources Laboratory (ARL) for the provision of the HYSPLIT
648 transport model (<http://www.ready.noaa.gov>).

649

650 **Reference**

651 Allan, J. D., Baumgardner, D., Raga, G. B., Mayol-Bracero, O. L., Morales-García, F., García-
652 García, F., Montero-Martínez, G., Borrmann, S., Schneider, J., Mertes, S., Walter, S., Gysel,
653 M., Dusek, U., Frank, G. P. and Krämer, M.: Clouds and aerosols in Puerto Rico - A new
654 evaluation, *Atmos. Chem. Phys.*, 8, 1293–1309, doi:10.5194/acp-8-1293-2008, 2008.

655 Baumgardner, D., Raga, G. B. and Muhlia, A.: Evidence for the formation of CCN by
656 photochemical processes in Mexico City, *Atmos. Environ.*, 38(3), 357–367,
657 doi:10.1016/j.atmosenv.2003.10.008, 2004.

658 Calvo, A. I., Baumgardner, D., Castro, A., Fernández-González, D., Vega-Maray, A. M.,
659 Valencia-Barrera, R. M., Oduber, F., Blanco-Alegre, C. and Fraile, R.: Daily behavior of urban
660 Fluorescing Aerosol Particles in northwest Spain, *Atmos. Environ.*, 184, 267–277,
661 doi:10.1016/j.atmosenv.2018.04.027, 2018.

662 Caulton E and Lacey M.: *Airborne Pollens and Spores. A Guide to Trapping and Counting*, 1st
663 ed., British Aerobiology Federation (BAF) Publishers, 1995.

664 Chi, M. C. and Li, C. S.: Fluorochrome in monitoring atmospheric bioaerosols and correlations
665 with meteorological factors and air pollutants, *Aerosol Sci. Technol.*, 41, 672–678,
666 doi:10.1080/02786820701383181, 2007.

667 Cziczo, D. J., Thomson, D. S., Thompson, T. L., DeMott, P. J. and Murphy, D. M.: Particle
668 analysis by laser mass spectrometry (PALMS) studies of ice nuclei and other low number
669 density particles, *Int. J. Mass Spectrom.*, 258, 21–29, doi:10.1016/j.ijms.2006.05.013, 2006.

670 Drewnick, F., Dall'Osto, M. and Harrison, R.: Characterization of aerosol particles from grass
671 mowing by joint deployment of ToF-AMS and ATOFMS instruments, *Atmos. Environ.*,
672 42(13), 3006–3017, doi:10.1016/j.atmosenv.2007.12.047, 2008.



- 673 Duan, J., Chen, Y. and Guo, X.: Characteristics of aerosol activation efficiency and aerosol and
674 CCN vertical distributions in North China, *Acta Meteorol. Sin.*, 26, 579–596,
675 doi:10.1007/s13351-012-0504-6, 2012.
- 676 Fennelly, M. J., Sewell, G., Prentice, M. B., O’Connor, D. J., and Sodeau, J. R.: The Use of
677 Real-Time Fluorescence Instrumentation to Monitor Ambient Primary Biological Aerosol
678 Particles (PBAP), *Atmosphere*, 9, 1–39, <https://doi.org/10.3390/atmos9010001>, 2017.
- 679 Gabey, A. M.: Laboratory and field characterization of fluorescent and primary biological
680 aerosol particles, Ph.D. thesis, University of Manchester, England, 2011.
- 681 Gabey, A. M., Gallagher, M. W., Whitehead, J., Dorsey, J. R., Kaye, P. H., and Stanley, W.
682 R.: Measurements and comparison of primary biological aerosol above and below a tropical
683 forest canopy using a dual channel fluorescence spectrometer, *Atmos. Chem. Phys.*, 10, 4453–
684 4466, doi:10.5194/acp-10-4453-2010, 2010.
- 685 Gabey, A. M., Vaitilingom, M., Freney, E., Boulon, J., Sellegri, K., Gallagher, M. W.,
686 Crawford, I. P., Robinson, N. H., Stanley, W. R., and Kaye, P. H.: Observations of fluorescent
687 and biological aerosol at a high-altitude site in central France, *Atmos. Chem. Phys.*, 13, 7415–
688 7428, <https://doi.org/10.5194/acp-13-7415-2013>, 2013.
- 689 Gioda, A., Mayol-Bracero, O. L., Scatena, F. N., Weathers, K. C., Mateus, V. L. and
690 McDowell, W. H.: Chemical constituents in clouds and rainwater in the Puerto Rican
691 rainforest: Potential sources and seasonal drivers, *Atmos. Environ.*, 68, 208–220,
692 doi:10.1016/j.atmosenv.2012.11.017, 2013.
- 693 Gosselin, M. I., Rathnayake, C. M., Crawford, I., Pöhlker, C., Fröhlich-Nowoisky, J., Schmer,
694 B., Després, V. R., Engling, G., Gallagher, M., Stone, E., Pöschl, U., and Huffman, J. A.:
695 Fluorescent bioaerosol particle, molecular tracer, and fungal spore concentrations during dry
696 and rainy periods in a semi-arid forest, *Atmos. Chem. Phys.*, 16, 15165–15184,
697 <https://doi.org/10.5194/acp-16-15165-2016>, 2016.
- 698 Healy, D. A., Huffman, J. A., O’Connor, D. J., Pöhlker, C., Pöschl, U., and Sodeau, J. R.:
699 Ambient measurements of biological aerosol particles near Killarney, Ireland: a comparison
700 between real-time fluorescence and microscopy techniques, *Atmos. Chem. Phys.*, 14, 8055–
701 8069, <https://doi.org/10.5194/acp-14-8055-2014>, 2014.



- 702 Hernandez, M., Perring, A. E., McCabe, K., Kok, G., Granger, G., and Baumgardner, D.:
703 Chamber catalogues of optical and fluorescent signatures distinguish bioaerosol classes,
704 *Atmos. Meas. Tech.*, 9, 3283–3292, <https://doi.org/10.5194/amt-9-3283-2016>, 2016.
- 705 Ho, J., Spence, M., and Hairston, P.: Measurement of Biological Aerosol with a Fluorescent
706 Aerodynamic Particle Sizer (FLAPS): Correlation of Optical Data with Biological Data,
707 *Aerobiologia*, 15, 281, <https://doi.org/10.1023/A:1007647522397>, 1999.
- 708 Huffman, J. A. and Santarpia, J. L.: Online techniques for quantification and characterization
709 of biological aerosol, in: *Microbiology of Aerosols*, edited by: Delort, A. M. and Amato, P.,
710 Wiley, Hoboken, NJ, chap. 1.4, 2017.
- 711 Kaye, P. H., Stanley, W. R., Hirst, E., Foot, E. V., Baxter, K. L., and Barrington, S. J.: Single
712 particle multichannel bio-aerosol fluorescence sensor, *Opt. Express*, 13, 3583–3593, 2005.
- 713 Kaye, P. H., Aptowicz, K., Chang, R. K., Foot, V., and Videen, G.: Angularly resolved elastic
714 scattering from airborne particles - Potential for characterizing, classifying, and identifying
715 individual aerosol particles, *Opt. Biol. Part.*, 238, 31–61, 2007.
- 716 Kulkarni, P., Baron, P. A. and Willeke, K.: *Aerosol Measurement: Principles, Techniques, and
717 Applications: Third Edition.*, 2011.
- 718 Möhler, O., DeMott, P. J., Vali, G., and Levin, Z.: Microbiology and atmospheric processes:
719 the role of biological particles in cloud physics, *Biogeosciences*, 4, 1059–1071,
720 [doi:10.5194/bg-4-10592007](https://doi.org/10.5194/bg-4-10592007), 2007.
- 721 Oliveira, M., Ribeiro, H. and Abreu, I.: Annual variation of fungal spores in atmosphere of
722 Porto: 2003, *Ann. Agric. Environ. Med.*, 12(2), 309–315, 2005.
- 723 Ortiz-Martínez, M. G., Rodríguez-Cotto, R. I., Ortiz-Rivera, M. A., Pluguez-Turull, C. W. and
724 Jiménez-Vélez, B. D.: Linking Endotoxins, African Dust PM₁₀ and Asthma in an Urban and
725 Rural Environment of Puerto Rico, *Mediators Inflamm.*, 2015, 784212,
726 [doi:10.1155/2015/784212](https://doi.org/10.1155/2015/784212), 2015.
- 727 Perring, A. E., Schwarz, J. P., Baumgardner, D., Hernandez, M. T., Spracklen, D. V., Heald,
728 C. L., Gao, R. S., Kok, G., McMeeking, G. R., McQuaid, J. B., and Fahey, D. W.: Airborne
729 observations of regional variation in fluorescent aerosol across the United States, *J. Geophys.
730 Res.-Atmos.*, 120, 1153–1170, <https://doi.org/10.1002/2014JD022495>, 2015.



- 731 Pope, F. D.: Pollen grains are efficient cloud condensation nuclei, *Environ. Res. Lett.*, 5,
732 044015, doi:10.1088/17489326/5/4/044015, 2010.
- 733 Quintero, E., Rivera-Mariani, F. and Bolaños-Rosero, B.: Analysis of environmental factors
734 and their effects on fungal spores in the atmosphere of a tropical urban area (San Juan, Puerto
735 Rico), *Aerobiologia (Bologna)*, 26, 113–124, doi:10.1007/s10453-009-9148-0, 2010.
- 736 Raga, G. B., Baumgardner, D. and Mayol-Bracero, O. L.: History of aerosol-cloud interactions
737 derived from observations in mountaintop clouds in Puerto Rico, *Aerosol Air Qual. Res.*,
738 16, 674–688, doi:10.4209/aaqr.2015.05.0359, 2016.
- 739 Roberts, G. C. and Nenes, A.: A Continuous-Flow Streamwise Thermal-Gradient CCN
740 Chamber for Atmospheric Measurements, *Aerosol Sci. Technol.*, 39, 206–221, 2005.
- 741 Rose, D., Gunthe, S. S., Mikhailov, E., Frank, G. P., Dusek, U., Andreae, M. O., and Pöschl,
742 U.: Calibration and measurement uncertainties of a continuous-flow cloud condensation nuclei
743 counter (DMT-CCNC): CCN activation of ammonium sulfate and sodium chloride aerosol
744 particles in theory and experiment, *Atmos. Chem. Phys.*, 8, 1153–1179,
745 <https://doi.org/10.5194/acp-8-1153-2008>, 2008.
- 746 Rivera-Mariani, F. E., Nazario-Jiménez, S., López-Malpica, F. and Bolaños-Rosero, B.:
747 Sensitization to airborne ascospores, basidiospores, and fungal fragments in allergic rhinitis
748 and asthmatic subjects in San Juan, Puerto Rico, *Int. Arch. Allergy Immunol.*, 155, 322-334,
749 doi:10.1159/000321610, 2011.
- 750 Rivera-Mariani, F. E., Almaguer, M., Aira, M. J. and Bolaños-Rosero, B.: Comparison of
751 atmospheric fungal spore concentrations between two main cities in the Caribbean basin, *P. R.*
752 *Health Sci. J.*, 39(3), 235–242, 2020.
- 753 Sarangi, B., Baumgardner, D., Bolaños-Rosero, B. and Mayol-Bracero, O. L.: Dataset to:
754 Measurement Report: An Exploratory Study of Fluorescence and CCN Activity of Urban
755 Aerosols in San Juan, Puerto Rico, Mendeley Data, Version 1, doi:10.17632/t26dctfk7t.1,
756 2021.
- 757 Savage, N. J., Krentz, C. E., Könemann, T., Han, T. T., Mainelis, G., Pöhlker, C. and Alex
758 Huffman, J.: Systematic characterization and fluorescence threshold strategies for the
759 wideband integrated bioaerosol sensor (WIBS) using size-resolved biological and interfering
760 particles, *Atmos. Meas. Tech.*, 10, 4279–4302, doi:10.5194/amt-10-4279-2017, 2017.



- 761 Spiegel, J. K., Buchmann, N., Mayol-Bracero, O. L., Cuadra-Rodriguez, L. A., Valle Díaz, C.
762 J., Prather, K. A., Mertes, S. and Eugster, W.: Do Cloud Properties in a Puerto Rican Tropical
763 Montane Cloud Forest Depend on Occurrence of Long-Range Transported African Dust?, *Pure*
764 *Appl. Geophys.*, 171(9), 2443–2459, <https://doi.org/10.1007/s00024-014-0830-y>, 2014.
- 765 Stanley, W. R., Kaye, P. H., Foot, V. E., Barrington, S. J., Gallagher, M. and Gabey, A.:
766 Continuous bioaerosol monitoring in a tropical environment using a UV fluorescence particle
767 spectrometer, *Atmos. Sci. Lett.*, 12, 195–199, doi:10.1002/asl.310, 2011.
- 768 Stolzenburg, M. R. and McMurry, P. H.: An Ultrafine Aerosol Condensation Nucleus Counter,
769 *Aerosol Sci. Tech.*, 14, 48–65, 1991.
- 770 Toprak, E. and Schnaiter, M.: Fluorescent biological aerosol particles measured with the
771 Waveband Integrated Bioaerosol Sensor WIBS-4: laboratory tests combined with a one year
772 field study, *Atmos. Chem. Phys.*, 13, 225–243, <https://doi.org/10.5194/acp-13-225-2013>, 2013.
- 773 Torres-Delgado, E., Baumgardner, D., and Mayol-Bracero, O. L.: Measurement Report:
774 Impact of African Aerosol Particles on Cloud Evolution in a Tropical Montane Cloud Forest
775 in the Caribbean, *Atmos. Chem. Phys. Discuss.* [preprint], [https://doi.org/10.5194/acp-2021-](https://doi.org/10.5194/acp-2021-88)
776 88, in review, 2021.
- 777 Twohy, C. H., McMeeking, G. R., DeMott, P. J., McCluskey, C. S., Hill, T. C. J., Burrows, S.
778 M., Kulkarni, G. R., Tanarhte, M., Kafle, D. N., and Toohey, D. W.: Abundance of fluorescent
779 biological aerosol particles at temperatures conducive to the formation of mixed-phase and
780 cirrus clouds, *Atmos. Chem. Phys.*, 16, 8205–8225, <https://doi.org/10.5194/acp-16-8205-2016>,
781 2016.
- 782 Valle-Díaz, C. J., Torres-Delgado, E., Colón-Santos, S. M., Lee, T., Collett, J. L., McDowell,
783 W. H., & Mayol-Bracero, O. L.: Impact of long-range transported african dust on cloud water
784 chemistry at a tropical montane cloud forest in Northeastern Puerto Rico. *Aerosol and Air*
785 *Quality Research*, 16(3), 653–664. doi.org/10.4209/aaqr.2015.05.0320, 2016.
- 786 Uin, J.: Ultra-High Sensitivity Aerosol Spectrometer (UHSAS) instrument handbook. ARM Tech. Rep.
787 DOE/SCARM-TR-163, USA, 17 pp., doi.org/10.2172/1251410, 2016.

788